CHAPTER

8

Dynamics of Charged Colloidal Suspensions Across the Freezing and Glass Transition

Hartmut Löwen

Dynamical correlations of charge-stabilized colloidal suspensions are investigated using Brownian dynamics simulations. Special emphasis is put on the kinetic glass transition in a charge-polydisperse suspension, and on long-time self-diffusion, particularly on a dynamical freezing rule for colloidal fluids. First, structural slowing down near the kinetic glass transition that shows up as a plateaulike behavior in the time-dependent density autocorrelation function is discussed for a supercooled polydisperse Yukawa fluid. Brownian dynamics results are compared with those of molecular dynamics, which ignores solvent effects. It is found that only the intermediate time region is affected by the different types of short-time dynamics, but the long-time behavior is at least qualitatively similar. Second, a dynamical scaling law at the freezing line of the fluid is empirically found stating that the ratio of long-time and short-time self-diffusion has a universal value close to 0.1. This constitutes a dynamical phenomenological freezing rule for colloidal suspensions, similar to the Lindemann melting criterion. Third, long-time translational and orientational diffusion is discussed for a system of Brownian hard spherocylinders. Along the fluid-crystal and fluid-nematic coexistence line, both long-time self-diffusion coefficients measured in terms of their short-time limits are nonmonotonic as a function of the length-to-width ratio of the spherocylinders. The ratio of long-time and short-time orientational self-diffusion is roughly 0.1, constituting a simple dynamical freezing rule for anisotropic fluids. For all topics, the connection to mode-coupling theories on the one hand, and to experiments on the other hand, is also briefly discussed.

8.1 Introduction

Suspensions of colloidal particles embedded in aqueous or some other organic solvent exhibit a local structure and a phase behavior that are highly reminiscent of those observed in simple atomic systems [1–4]. In contrast to atomic systems, however, the length scale of structural ordering is *mesoscopic* roughly determined by the mean interparticle spacing $\ell = n_p^{-1/3}$, where n_p is the particle concentration. This permits a direct visualization of the particle positions using direct image processing methods or video microscopy and opens a fascinating way to see and measure structural and dynamical correlations in real space; see for example, [5]. If the colloidal particles are practically monodisperse spheres, they serve as ideal realizations of simple model liquids from classical statistical mechanics. Two major interaction models have frequently been applied to describe the interaction between index-matched colloidal particles: the hard-sphere model and the Yukawa model. For *sterically stabilized* suspensions, a simple hard-sphere pair interaction simply incorporating the excluded volume of the spheres can be employed. For an interparticle separation r the potential energy between two particles is then given by

$$U(r) = \begin{cases} 0, & \text{for } r \geq d \\ \infty, & \text{for } r < d \end{cases} \tag{8.1}$$

where d is the diameter of the particles. For *charge-stabilized* suspensions, on the other hand, Derjaguin, Landau, Verwey, and Overbeek (DLVO) [6, 7] have calculated that at infinite dilution the effective interaction is pairwise and of the Yukawa type

$$U(r) = \frac{(Z_{\text{eff}}e)^2}{4\pi\epsilon_0\epsilon r}\exp(-\kappa r) \tag{8.2}$$

with

$$Z_{\text{eff}} = Z\exp(\kappa d/2)/(1+\kappa d/2) \tag{8.3}$$

Ze denoting the bare charge of the colloidal "macroions" and

$$\kappa = (\sum_i n_i z_i^2/k_B T\epsilon_0\epsilon)^{1/2} \tag{8.4}$$

being the inverse Debye-Hückel screening length. Here n_i and z_i are the concentration and charge of the ith type of impurity ion (including the counterions) in the solvent and T is the temperature. A Poisson-Boltzmann-cell model designed for strongly interacting macroions also results in an effective Yukawa interaction [8]. A more refined ab initio study of the "primitive model," which includes counter- and impurity-induced effective many-body forces between the macroions [9, 10] indeed reveals that the Yukawa-pair-interaction remains a satisfying description of the effective macroionic forces [11]. These calculations show that the Yukawa picture is justified even for high concentrations provided the packing fraction

of the macroions is not too high. However, the actual values of the parameters Z_{eff} and κ entering into Eq. (8.2) have to be renormalized with respect to the DLVO predictions Eqs. (8.3) and (8.4) valid at infinite dilution. In order to check the charge renormalization, it is highly motivated to study structural and dynamical quantities for Yukawa systems by theory and computer simulations and to compare with the experimental data gained from charge-stabilized colloidal suspensions.

The special purpose of this chapter is to study the *dynamics* of Yukawa systems, particularly in the neighborhood of *phase transitions*. In contrast to atomic and molecular fluids whose dynamics are Newtonian, the complete time-scale separation between solvent and colloidal particle relaxation leads to irreversible Brownian motion of the macroparticles in the solvent. For dilute systems, these dynamics can explicitly be obtained by writing the finite-difference version of the particle displacements as follows: We consider N particles confined to a large volume V with positions $\{\mathbf{r}_i : i = 1, \ldots, N\}$. The particle positions after a small time step Δt are gained from those at time t by the formula [12, 13]:

$$\mathbf{r}_i(t+\Delta t) = \mathbf{r}_i(t) + \frac{1}{\xi}\mathbf{F}_i(t)\Delta t + (\Delta\mathbf{r})_R + O(\Delta t^2) \tag{8.5}$$

where the random displacement $(\Delta\mathbf{r})_R$ is sampled from a Gaussian distribution of zero mean, $\overline{(\Delta\mathbf{r})_R} = 0$, and variance $\overline{(\Delta\mathbf{r})_R^2} = 6k_BT\Delta t/\xi$. Here $F_i(t)$ are the total forces on the particles derived from the pairwise interaction Eq. (8.1) or (8.2), and $\xi = 3\pi\eta d$ is the solvent friction coefficient (η denoting the solvent shear viscosity), which is related to the short-time diffusion constant as follows:

$$D_0 = k_BT/\xi \tag{8.6}$$

D_0 provides a natural scale to measure the long-time diffusion coefficient D_L defined by

$$D_L = \lim_{t\to\infty}\left(\frac{1}{6t}\left\langle\sum_{j=1}^{N}\frac{1}{N}[\mathbf{r}_i(t)-\mathbf{r}_i(0)]^2\right\rangle\right) \tag{8.7}$$

where $< \cdots >$ denotes a canonical average. We remark that Eq. (8.5) also constitutes a direct algorithm for a Brownian dynamics computer simulation. In concentrated colloidal systems, *hydrodynamic forces* induced by the solvent are relevant. In principle, these could be approximately included by replacing ξ by a $3N \times 3N$ matrix depending parametrically on the positions $\{\mathbf{r}_i\}$. In the following, however, also for simplicity, we take ξ to be diagonal and constant, thus neglecting any hydrodynamic interactions, which is a reasonable assumption for dilute though highly interacting charged suspensions.

As regards phase transformations, several types of phase transitions are conceivable. The best known is the *freezing transition* [4]. The hard-sphere fluid exhibits a strong first-order freezing transition into a dense-packed crystal with a large density jump of about 10%. Also the Yukawa fluid freezes into a BCC or FCC crystal depending on whether the interaction is soft (small κ) or harsh.

Another transition is the kinetic *glass transition* of an undercooled or compressed fluid. This is not a true thermodynamic phase transition with a non analyticity in the free energy but a smooth transition of dynamical origin where time-dependent correlations decay only for very long times.

This chapter is concerned with dynamical signatures at the freezing and fluid-to glass transition of a charged colloidal suspension. Near the glass transition the long-time self-diffusion coefficient D_L practically drops to zero, exhibiting a power law as a function of a typical parameter measuring the distance to the glass transition point. One main point of this chapter is to check explicitly the validity of this power law by performing extensive Brownian dynamics computer simulations for a charge-polydisperse colloidal suspension [14]. Also the relaxation of the density autocorrelation function is studied in order to detect the kinetic glass transition by simple dynamical diagnostics. Particularly, the scenario of the kinetic glass transition is compared to that of a system governed by Newtonian dynamics. It is found that the long-time relaxation is very similar but the short-time and intermediate-time relaxation is different.

At the freezing transition, the long-time self-diffusion coefficient D_L jumps from a finite value at the fluid side of the phase coexistence line to a very small value corresponding to diffusion of grain boundaries and vacancies in the crystalline phase. Interestingly enough, Löwen et al. [15] found that the ratio D_L/D_0 exhibits a *universality* at the fluid coexistence line. It always equals 0.098 at the freezing transition of the fluid regardless of the interaction between the colloidal particles. This constitutes a dynamical phenomenological freezing rule, similar in spirit to the Lindemann rule [16] of melting or the Hansen-Verlet [17] freezing rule which have proved to be very helpful in estimating fluid-solid coexistence lines. As early as 1910 Lindemann [16] put forward the empirical fact that the ratio of the root-mean-square displacement and the average interparticle distance at the solid melting line has a value of roughly 0.15. The Hansen-Verlet criterion [17] states that the amplitude of the first maximum of the liquid structure factor has a universal value of $\simeq 2.85$ along the liquid freezing line. The Hansen-Verlet and the dynamical freezing criterion of Löwen et al. [15] are universal in the sense that they do not depend on the detailed nature of the spherical interaction potential.

It is interesting to check whether the concept of dynamical universality at the freezing line of the fluid also holds for *anisotropic fluids* where one has coexisting crystalline or nematic phases. In order to clear that up, we report Brownian dynamics simulations of hard spherocylinders for different total length-to-width ratios p_c. As a result the orientational self-diffusion coefficient measured in terms of it short-time limit also drops one order of magnitude at the fluid-liquid-crystalline transition line. The actual value, however, depends a bit on p_c; hence the self-diffusion is not that universal as in the case of isotropic interactions.

The chapter is organized as follows: First we discuss Brownian dynamics of a supercooled charge-polydisperse Yukawa fluid near the kinetic glass transition in Section 8.2. Then we turn to self-diffusion at the fluid freezing line in Section 8.3. For both topics, the experimental and theoretical situation is first briefly reviewed

and then computer simulation results are discussed. Section 8.4 is devoted to self-diffusion in anisotropic fluids. We state some open problems in Section 8.5.

8.2 Kinetic Glass Transition in Colloidal Suspensions

In this section we review some recent experimental theoretical and simulational results for the kinetic glass transition in colloidal suspensions. The main emphasis is placed on results from a Brownian dynamics computer simulation.

8.2.1 Light Scattering Experiments

Pusey, van Megen, and co-workers [18-22] measured the time-dependent density autocorrelation function over a broad time window for a sterically stabilized colloidal suspension as a function of the packing fraction of the particles. The experimental method they used was dynamical light scattering. Despite the enormous differences in time scales between atomic and mesoscopic glass formers, the supercooled colloidal liquid exhibits qualitative features very similar to that of an atomic liquid at the kinetic glass transition. The advantage for interpretation is that the experimental system is a rather simple: It represents a hard-sphere-like system with a small polydispersity.

Also the relaxation of spherical polystyrene micronetwork particles of mesoscopic size, swollen in a good solvent, was recently measured over a very broad time window by Bartsch and co-workers [23-25], representing another type of colloidal suspension. The samples are a bit more polydisperse ($p_\sigma = 0.16$) than that used by van Megen and co-workers; consequently the glass transition occurred at higher volume fractions of the colloidal spheres. Again the long-time relaxation was found to be very similar to that of simple atomic liquids. Charge-stabilized colloidal suspensions also form glasses; experimental studies at the glass transition were done by Sirota et al. [26] and Meller and Stavans [27].

It would be interesting to apply real-space methods by tagging a single particle and following its way using video microscopy. Then one could link the results more easily to computer simulations. Also most of the concepts and jargon concerning the relaxation of the kinetic glass transition (like particle cage relaxation and thermally activated hopping) are borrowed from real-space pictures and should be tested experimentally.

8.2.2 Theory

The most prominent theory of the glass transition capable of making nontrivial predictions for the relaxation scenario is the mode-coupling theory (MCT) developed by Götze and co-workers [28]. The experimental results of van Megen and Pusey [19] were compared with predictions of mode-coupling theory for a hard-sphere system by Götze and Sjögren [29] and by Fuchs et al. [30]; good agreement was found between mode-coupling theory and the experimental data.

The MCT was originally derived for molecular dynamics. It was shown explicitly by Szamel and Löwen [31] that the asymptotic predictions of MCT do not change for Brownian dynamics. Hence, within MCT, the asymptotics of the density relaxation are universal with respect to the short-time dynamics. For example, the ideal glass transition occurs at the same temperature for MD and BD. There have only been a few attempts to incorporate hydrodynamic interactions into MCT, a first step having been done by Fuchs [32]. Again the asymptotic scenario remains unaffected by the explicit form of the hydrodynamic interactions, while there are changes for finite times.

Recently, Kawasaki [33] proposed a stochastic model particularly designed for the Brownian dynamics of colloidal suspensions. Here also activated hopping is incorporated in some sense into the theory.

8.2.3 Brownian Dynamics Simulations

In order to make a direct comparison between undercooled atomic and colloidal fluids, Löwen et al. [34] performed an extensive simulation for a charge-stabilized polydisperse colloidal suspension near the kinetic glass transition for both Brownian and Newtonian dynamics. To date this is the only simulation for the kinetic glass transition which takes solvent friction into account. It may be mentioned that there are other Monte Carlo simulations of the glass transition which interprete the fictitious Monte Carlo move dynamics as a real dynamics; see for example [35]. If the long-time behavior is independent with respect to short-time dynamics, then one can chose one suitable fictitious dynamics to extract the long-time dynamics such that the actual computational time to explore sufficient statistics is smaller. An idea of this kind was used by Kob et al. [36, 37].

As a model system, a charge-polydisperse colloidal fluid, described by the potential

$$U_{ij}(r) = U_0 \frac{\ell}{r} \frac{Z_i Z_j}{\bar{Z}^2} \exp\left(-\kappa^* \frac{r-\ell}{\ell}\right) \tag{8.8}$$

was chosen in Ref. [34] where $\kappa^* \equiv \kappa\ell \equiv 7$ and $n_p \equiv \ell^{-3}$ are fixed. The system is then cooled from a temperature $T^* \equiv k_B T/U_0 = 0.45$ down to $T^* = 0.10$. The macroionic charges $\{Z_i : i = 1, \ldots, N\}$ are continuously distributed according to a Schultz distribution with a relative charge polydispersity of 0.5. The characteristic time scales for BD and MD are $\tau_B = \xi\ell^2/U_0$ for Brownian and $\tau_N = \sqrt{m\ell^2/U_0}$ for Newtonian dynamics, where m is the mass of the particle. The high value of κ^* chosen implies that the system behaves similar to a polydisperse hard-sphere system. In order to perform an explicit mapping from the charge-polydisperse onto a size-polydisperse system by using the Gibbs-Bogoliubov inequality, an effective relative size polydispersity of about 0.13 was obtained [34]. Thus the data correspond roughly to those of the experiments of Bartsch et al. [23-25]. Although more complicated than a monodisperse model,

the motivation for the charge-polydisperse model is twofold: First, crystallization is suppressed, and one is sure to encounter a glassy state in the simulations. Second, polydispersity is an intrinsic property of any colloidal suspension, and it is thus natural to incorporate it into the theoretical model directly.

The dynamical key quantities characterizing the glass transition are the density autocorrelation functions in real space as well as in Fourier space. We define the general density autocorrelation function as follows

$$C_\rho(t) \equiv C_\rho(\mathbf{r}, \mathbf{r}', t) = \left\langle \sum_{i,j=1}^{N} \delta(\mathbf{r} - \mathbf{r}_j(0))\ \delta(\mathbf{r}' - \mathbf{r}_i(t)) \right\rangle \tag{8.9}$$

This can be split into a self (s) and distinct (d) part

$$C_\rho(\mathbf{r}, \mathbf{r}', t) = C_\rho^{(s)}(\mathbf{r}, \mathbf{r}', t) + C_\rho^{(d)}(\mathbf{r}, \mathbf{r}', t) \tag{8.10}$$

with

$$C_\rho^{(s)}(\mathbf{r}, \mathbf{r}', t) = \left\langle \sum_{j=1}^{N} \delta(\mathbf{r} - \mathbf{r}_j(0))\ \delta(\mathbf{r}' - \mathbf{r}_j(t)) \right\rangle \tag{8.11}$$

$$C_\rho^{(d)}(\mathbf{r}, \mathbf{r}', t) = \left\langle \sum_{i\neq j=1}^{N} \delta(\mathbf{r} - \mathbf{r}_j(0))\ \delta(\mathbf{r}' - \mathbf{r}_i(t)) \right\rangle \tag{8.12}$$

$C_\rho^{(s)}(\mathbf{r}, \mathbf{r}', t)$ [resp., $C_\rho^{(d)}(\mathbf{r}, \mathbf{r}', t)$] give the joint probability density to find a particle at position $\mathbf{r}'$ after a time t and the same (resp. another) particle at position $\mathbf{r}$ for zero time.

By normalization, we obtain the *van Hove correlation function*

$$G(\mathbf{r}, \mathbf{r}', t) = C_\rho(\mathbf{r}, \mathbf{r}', t)/n_p^2 \tag{8.13}$$

that also naturally splits into a self- and distinct part

$$G(\mathbf{r}, \mathbf{r}', t) = G_s(\mathbf{r}, \mathbf{r}', t) + G_d(\mathbf{r}, \mathbf{r}', t) \tag{8.14}$$

The distinct part of the van Hove correlation function is the time-dependent generalization of the pair distribution function $g(r)$

$$G_d(r, t) = \frac{1}{n_p N} \left\langle \sum_{i\neq j=1}^{N} \delta(\mathbf{r} - \mathbf{r}_i(0) + \mathbf{r}_j(t)) \right\rangle \tag{8.15}$$

Of course, $G_d(r, 0) = g(r)$ and $\lim_{t\to\infty} G_d(r, t) = 1$ in a fluid, whereas the van Hove function has frozen-in components for large times in a glass. The self-part reads:

$$G_s(r, t) = \frac{1}{n_p N} \left\langle \sum_{j=1}^{N} \delta(\mathbf{r} - \mathbf{r}_j(0) + \mathbf{r}_j(t)) \right\rangle \tag{8.16}$$

For $t = 0$, we get $G_s(r, 0) = \delta(\mathbf{r})/n_p$, and the long-time limit is given by the hydrodynamic behavior

$$G_s(r, t) \cong \frac{1}{n_p}(4\pi D_L t)^{3/2} \exp(-r^2/4D_L t) \tag{8.17}$$

Furthermore, one can take the Fourier transform of $G_s(r, t)$ and $G_d(r, t)$ with respect to r to gain corresponding Q-dependent structure factors $S_s(Q, t)$, $S_d(Q, t)$ that are defined as

$$S_s(Q, t) = \frac{1}{n_p N} \sum_{j=1}^{N} \left\langle \exp\{i\mathbf{Q} \cdot [\mathbf{r}_j(t) - \mathbf{r}_j(0)]\} \right\rangle \tag{8.18}$$

$$S_d(Q, t) = \frac{1}{n_p N} \sum_{\ell \neq j=1}^{N} \left\langle \exp\{i\mathbf{Q} \cdot [\mathbf{r}_j(t) - \mathbf{r}_\ell(0)]\} \right\rangle \tag{8.19}$$

It is clear that $S_d(Q, 0) = S(Q)$; that is, $S_d(Q, t)$ equals the static structure factor for $t = 0$. Further Fourier transformation with respect to time t then leads to the dynamical structure factors $S_s(Q, \omega)$, $S_d(Q, \omega)$. The latter quantity is directly accessible in dynamical scattering experiments.

As a first dynamical diagnostic for the kinetic glass transition, only the relaxation of the self-part of the van Hove function, $G_s(r, t)$, can be used. As the system is gently cooled down further, there is a sudden drastic change in the relaxation. The function $r^2 G_s(r, t)$ now shows the buildup of a secondary peak roughly at a mean particle distance ℓ, whereas the position of the first peak remains frozen over "long" (i.e., $100\tau_B$, τ_N) times. This is shown in Fig. 8.1, where $r^2 G_s(r, t)$ is plotted above and near the kinetic glass transition for Brownian dynamics (BD). Hence we have a first indication that hopping processes do occur. Of course this qualitative change occurs gradually in a smooth manner but still in a relatively narrow temperature interval, and it can be used to determine an estimate for the kinetic glass transition, which is now microscopically connected with a change in the relaxation behavior from hydrodynamic relaxation to relaxation by thermally activated jumps. Remarkably, the temperature interval in which this dynamical crossover occurs is the same for BD and molecular dynamics (MD). Also the buildup of the secondary peak is present in BD, indicating that there is the *same* crossover to thermally activated jumps in the Brownian case although there are no phonons present in the Brownian case. By this diagnostics one may estimate the temperature for the kinetic glass transition for both MD and BD to be within

$$0.115 < T^*_{\text{glass}} < 0.12. \tag{8.20}$$

The long-time diffusion constant drops to very small values near T^*_{glass} and a power law with a small residual contribution ΔD due to jumps fits well the data of the supercooled liquid

$$D_L = \Delta D + A(T^* - T^*_{\text{glass}})^\gamma \tag{8.21}$$

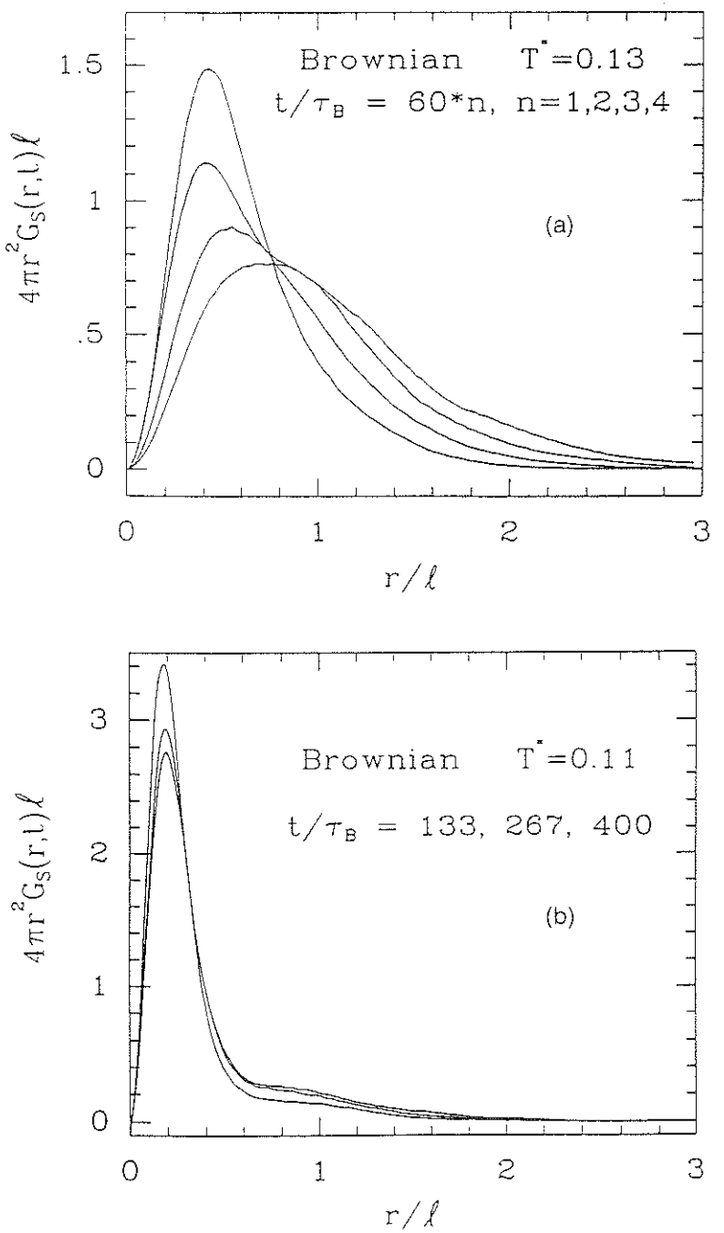

Figure 8.1 Self-part of the van Hove function $G_s(r, t)$ multiplied by $4\pi r^2 \ell$ versus reduced distance r/ℓ calculated with Brownian dynamics; the curves from left to right (or top to bottom) are for increasing time arguments. (a) Results for $T^* = 0.13$ and $t^* = t/\tau_B = 60, 120, 180, 240$. (b) Results for $T^* = 0.11$ and $t^* = 133, 267, 400$. From Ref. [34].

with $\gamma \approx 1.4$ for *both* BD and MD. Plots of the long-time self-diffusion constant as a function of $T^* - T^*_{\text{glass}}$ are shown in Fig. 8.2. On a double logarithmic plot the values D_L fall on a straight line, indicating the validity of the power law [Eq. (8.21)].

Another interesting quantity is the distinct part of the van Hove function, $G_d(r, t)$, defined in Eq. (8.15). At the kinetic glass transition, it turns out, again both for BD and MD, that a peak at $r = 0$ is built up, giving again strong evidence for particle-exchange hopping processes. In a dense supercooled liquid, however, these processes are more complicated than simple pair exchanges. In general, more than two particles (small clusters of particles) participate to a real position-exchange process; see for example, Migayawa et al. [38].

The other interesting quantities are the spatial and time Fourier transformations of $G_s(r, t)$ and $G_d(r, t)$. In Fig. 8.3, $S_s(Q, t)$ is plotted as a function of time t on a logarithmic scale for a fixed wave vector Q near the first peak of the static structure factor $S(Q)$. From this figure it becomes evident that there are qualitative different relaxations for BD and MD. For short times t/τ_N, t/τ_B, the decay of the density

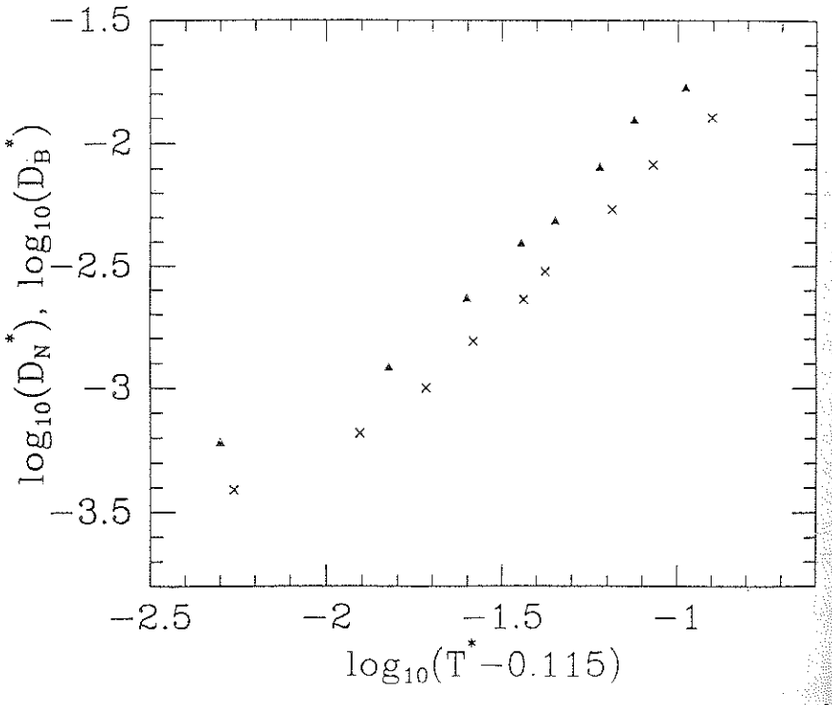

Figure 8.2 Double logaritmic plot of the reduced diffusion constants $D^*_N = D_L\tau_N/\ell^2$ (Newtonian dynamics, crosses) and $D^*_B = D_L\tau_B/\ell^2$ (Brownian dynamics, triangles) versus distance $T^* - 0.115$ to the kinetic glass transition. From Ref. [34].

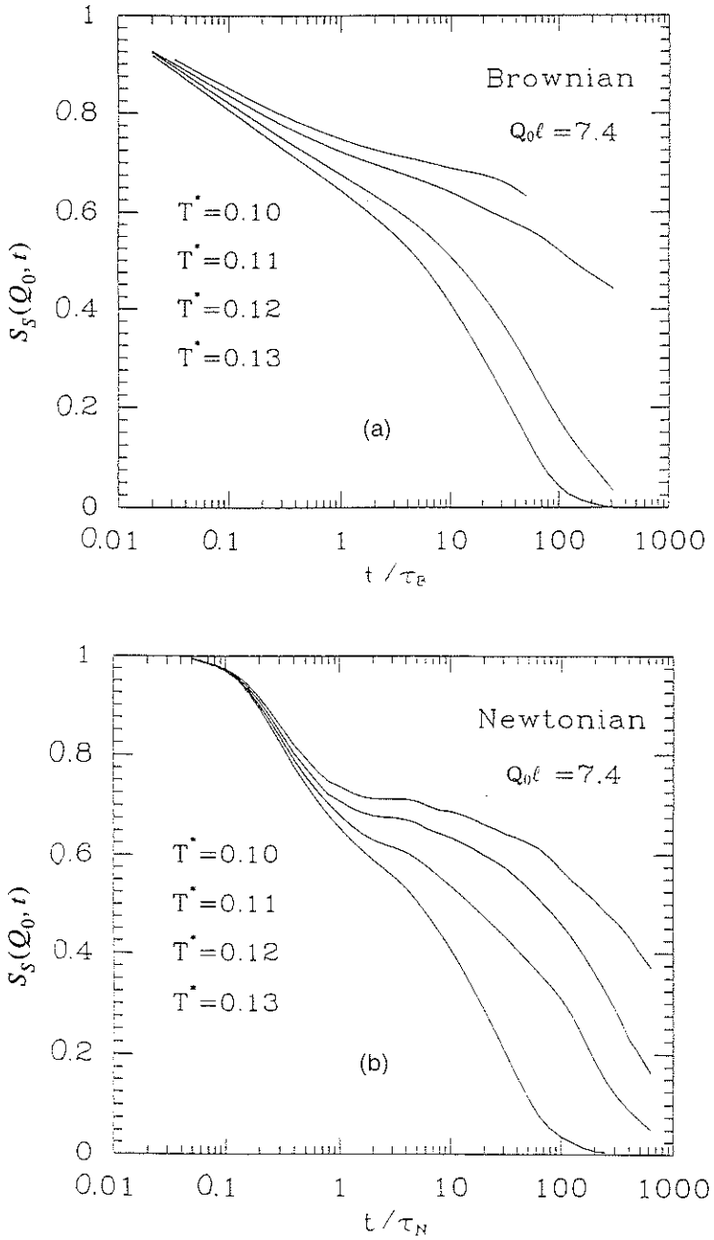

Figure 8.3 Self-part of the density autocorrelation function $S_s(Q, t)$ versus reduced time $t^* = t/\tau_N$, t/τ_B (on a logarithmic scale) for $Q = Q_0 = 7.4/\ell$ and (from bottom to top) $T^* = 0.13$, 0.12, 0.11, and 0.10. (a) Brownian dynamics; (b) molecular dynamics. From Ref. [34].

autocorrelation function is different. It starts with $1 - \mathcal{O}(t^2)$ in the MD and with $1 - \mathcal{O}(t)$ in the BD case. For very long times, $S_s(Q, t)$ and $S_d(Q, t)$ can be fitted by a stretched exponential law $\sim \exp[-(t/t_0)^\nu]$, where t_0 is strongly temperature dependent and, as ν, also depends on Q. The exponent ν is found to be practically the same for BD as for MD. So the α-relaxation scenario is quite similar. From Fig. 8.3 it becomes clear that, for times small compared to α-relaxation but still larger than τ_B, τ_N, there are qualitative differences; that is, the different short-time behavior also induces a different crossover to the long-time behavior. The decay is smoother in the BD case, and there is no clear indication for a buildup of a plateau near T^*_{glass}. (Of course, for smaller temperatures there must be a quasiplateau.) If one looks at the time Fourier transforms of $S_d(Q, t)$ or $S_s(Q, t)$ (at $\kappa^* = 7$), one finds that there is a shoulder at the corresponding frequency for MD that is missing for BD. It is tempting to call this a β relaxation, and one main conclusion is that the dynamical onset of β-relaxation is qualitatively different for BD and MD. In mode-coupling theory, β-relaxation is defined in a different way, namely, by an additional scaling law near T^*_{glass} whose asymptotic behavior can be studied analytically. Again, mode coupling theory predicts no difference for MD and BD in the asymptotic case. The difference obtained in the simulation, however, occurs for smaller times that are not yet in the asymptotic regime.

Summarizing, the kinetic glass transition manifests itself microscopically as a crossover from hydrodynamic relaxation to relaxation by thermally activated jumps. This crossover is not completely sharp but occurs on a very narrow temperature interval upon cooling. The transition temperature is the same for BD and MD. The dynamical onset of β-relaxation, however, is different. A shoulder in the dynamical structure factor at intermediate frequencies is present for MD but missing for BD. On the other hand, α-relaxation is similar, supporting the prediction of simple mode-coupling theory.

We finally note that a detailed analysis has also been made distinguishing between low-charge and high-charge particles [39]. As expected, the high-charge particles freeze first and then the low-charge particles follow, but everything happens in a smooth manner. The kinetic glass transition is connected with a considerable change in the ratio of the long-time self-diffusion coefficients for the low-charge and high-charge particles.

8.3 Long-Time Self-Diffusion Across the Freezing Transition

In this section we review some recent experiments, theories, and simulations of the long-time self-diffusion coefficient for a Brownian Yukawa system viz. charge-stabilized colloidal suspension and also sterically stabilized suspension.

8.3.1 Measurements of the Long-Time Self-Diffusion Coefficient

Different experimental techniques have been used to measure the long-time self-diffusion coefficient D_L. Most of the studies have used dynamical light scattering [40-49]. This technique, however, may have problems with multiple scattering for concentrated colloidal suspensions. Next also more refined methods where some particle are dyed have been applied as forced Rayleigh scattering [50, 51, 15] and fluorescence recovery after photobleaching [52, 53]. Finally fiber-optical quasielastic light scattering, where multiple scattering effects are negligible [54], and pulsed-field NMR [55] experiments were performed. It has to be pointed out that the error obtained in using the different experimental methods is still large, lying on the 10% level for concentrated or strongly interacting suspensions.

In Refs. [15] and [51] D_L/D_0 was measured close to the freezing transitions of a charged colloidal suspension for different salt concentrations. It was found that the ratio D_L/D_0 equals 0.1 on the fluid freezing line. Also in Ref. [51] D_L/D_0 was systematically investigated across the freezing transition involving diffusion in the compressed fluid, which is finite and very similar to the usual fluid diffusion and diffusion in the solid phase which is much slower and results from vacancy hopping and grain boundary diffusion.

8.3.2 Theories for the Long-Time Self-Diffusion Coefficient in Strongly Interacting Colloidal Suspensions

In most of the theoretical approaches to the long-time self-diffusion coefficient in concentrated suspensions hydrodynamic interactions are neglected completely. Historically the first approach is the mode-coupling theory, which was developed by Mori and Zwanzig [56] and applied to colloids by Hess and Klein [57]. Its starting point is the exact expression for the tagged particle intermediate scattering function. This expression is then analyzed and approximated using ideas borrowed from the mode-coupling theories of simple liquids. The final result is a nonlinear self-consistent equation for the scattering function. This equation also involves the collective scattering function $S_d(Q, t)$, for which another self-consistent equation is written down. As nonlinear self-consistent equations are difficult to solve, one usually approximates them further, introducing short-time limits of the scattering functions into friction kernels (for details, see [57-59] and references cited therein). In this way one obtains the following expression for D_L:

$$\frac{D_L}{D_0} = \left(1 + \frac{1}{6\pi^2 n_p} \int_0^\infty \mathrm{d}Q\, Q^2 \frac{[S(Q) - 1]^2}{1 + S(Q)}\right)^{-1} \tag{8.22}$$

Another theory has been proposed by Medina-Noyola [60]. It is based on a analysis of the generalized Langevin equation describing the coupled motion of

the tagged particle and the surrounding colloidal suspension. The final result for D_L is:

$$D_L/D_0 = \left(1 + \frac{n_p}{6}\int \mathrm{d}r\,[g(r)-1]^2\right)^{-1} \tag{8.23}$$

It turns out that numerically the Eqs. (8.22) and (8.23) are very close. These also provide a very simple explanation for the observed universality at the fluid freezing line: Since $S(Q)$ is universal at freezing provided Q is scaled by $n_p^{1/3}$ according to the Hansen-Verlet rule (see, e.g., [61]), D_L/D_0 also has to be invariant at the fluid freezing transition. This theoretical justification is, however, too simple since the theories do only work at high dilution. Indeed the actual value of D_L/D_0 is 0.3; hence it is strongly overestimated by theory.

More sophisticated theories also designed for concentrated suspensions are the modified Enskog approach proposed by Cichocki [62] and investigated by Löwen and Szamel [63] and the Enskog approach first used by Szamel and Leegwater [64, 65] for hard spheres, which was then generalized to the soft Yukawa potential [63]. These approaches involve the particle interaction potential explicitly and do not give universality at freezing. However, these actually give better absolute values than the former theories for high concentrations. In Figs. 8.4 to 8.6 we

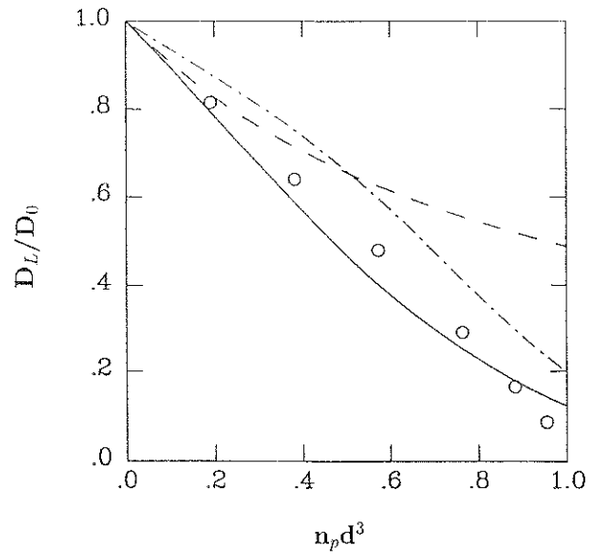

Figure 8.4 Long-time self-diffusion coefficient divided by its low-density limit, D_L/D_0, as a function of the reduced density $n_p d^3$ for a hard-sphere suspension. Circles: Brownian dynamics data of Ref. [68]; solid line: Enskog theory; dashed line: modified Enskog theory; dot-dashed line: theory of Medina-Noyola, Eq.(23). From Ref. [63].

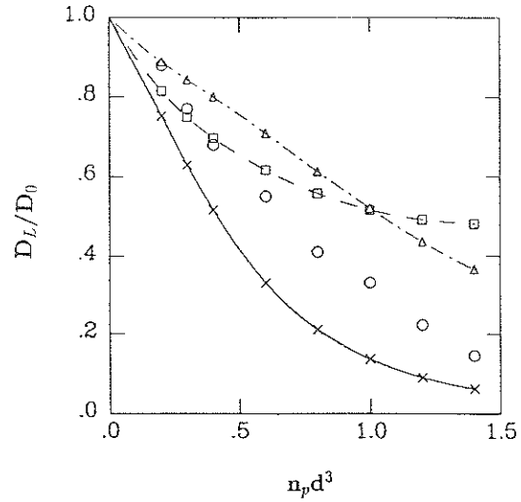

Figure 8.5 Self-diffusion coefficient divided by its low-density limit, D_L/D_0, as a function of the reduced density $n_p \ell^3$ for a Yukawa suspension where the Yukawa potential is written as $U(r) = U_0(\ell/r)\exp[-\kappa^*(r-\ell)/\ell]$. The parameters of the Yukawa potential are $\kappa^* = 8$, $k_BT/U_0 = 1$. Circles: Brownian dynamics results; crosses: Enskog theory; squares: modified Enskog theory; triangles: theory of Medina-Noyola, Eq. (8.23). Lines serve only as guides to the eyes; the actual calculations were performed at the data points. From Ref. [63].

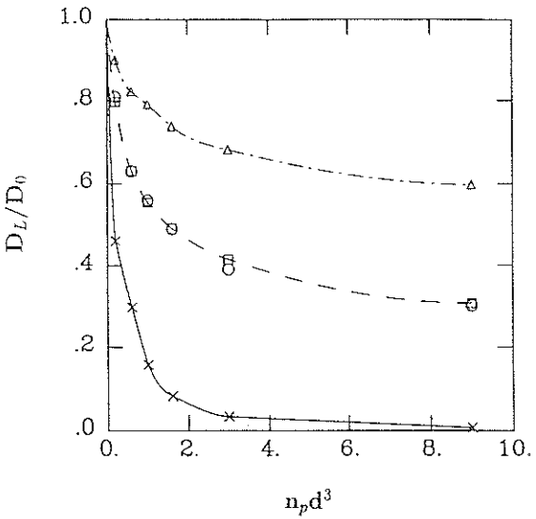

Figure 8.6 Same as Fig. 8.5; but now for a softer Yukawa potential with parameters $\kappa^* = 3$, $k_BT/U_0 = 0.8$. From Ref. [63].

have shown the results for D_L/D_0 for different theories and the "exact" computer simulational results for varying particle concentration from the dilute limit to high concentrations near the fluid freezing point. A hard-sphere system was taken in Fig. 8.4, while two different Yukawa interactions were assumed for Figs. 8.5 and 8.6. For hard spheres the Enskog description gives satisfactory results, while the modified Enskog theory fails. For a soft Yukawa interaction, on the other hand, the Enskog theory fails, and its modification works well. Medina-Noyola's expression always fails for large concentrations. Consequently, at the moment, there is no satisfactory theory that works for both soft and hard interactions at low and high concentrations. Recently, Indrani and Ramaswamy [66] used a self-consistent mode-coupling approach to check the universality of D_L/D_0 at freezing. Their values of ≈ 0.05 also seem to be too low as compared to the computer simulation and experimental value of 0.1.

8.3.3 Computer Simulations of the Long-Time Self-Diffusion Coefficient

In the fluid phase, the ratio D_L/D_0 of the hard-sphere system with simple Brownian dynamics given by Eq. (8.5) has been "exactly" calculated by Brownian dynamics simulations by Cichocki and Hinsen [67, 68] and for the Yukawa system by Löwen et al. [63, 69]. The main problem is the finite time window, where the extrapolation to infinite times is somewhat arbitrary. One can use the exact solution for hard spheres in the semidilute limit to find an explicit long-time extrapolation [68] or fit to a stretched exponential or some other function. The resulting values of D_L/D_0 change by about 5% and are thus fortunately rather insensitive to the extrapolation procedure, while the decay time to the asymptotic diffusive behavior depends much more on the extrapolation scheme. Computer simulation results are desirable since they provide an exact test of existing theories and are the basis of comparing experimental data with results from theoretical models for the colloidal interaction [69].

In the following we give some analytical fit formulae [69, 70] for the simulation results that are helpful for a simple comparison with experimental and theoretical data.

Hard Spheres

A hard-sphere system is characterized solely by its packing fraction $\phi = \pi n_p d^3/6$. A simple formula for D_L/D_0 is

$$D_L/D_0 = 1 - 1.94\phi + 1.25\phi^2 - 2.042\phi^3 \tag{8.24}$$

This equation is valid for any ϕ in the fluid phase (i.e., $\phi < 0.494$) and has a relative error of less than 3%. The exact low-density limit $D_L/D_0 = 1 - 2\phi + O(\phi^2)$ is only approximately incorporated into Eq. (24). At the fluid freezing point ($\phi = 0.494$), we get $D_L/D_0 = 0.100$ from Eq. (8.24), which is practically identical to the universal value of 0.098 obtained from the simulations [68, 15].

Yukawa Fluids

We write the Yukawa potential as

$$U(r) = U_0 \ell \exp(\kappa^*) \exp(-\kappa r)/r \tag{8.25}$$

where U_0 is an energy and $1/\kappa$ the length scale. The only relevant dimensionless parameters [71] are κ^* and T^*. This means that D_L/D_0 does only depend on the two parameters T^* and κ^*. The fit formula for D_L/D_0 reads as

$$\begin{aligned} D_L/D_0 &= 0.6457 \exp(-2.3429 t_r) \\ &\quad + 0.3183 \exp[-(31.70 + 6.053\kappa^*)t_r] + 0.03598 \end{aligned} \tag{8.26}$$

Here t_r is the ratio of the freezing temperature to the actual temperature

$$t_r = T^*_{\text{freez}}(\kappa^*)/T^* \tag{8.27}$$

Meijer and Frenkel have calculated the fluid freezing line in the (T^*, κ^*)-diagram [71]. Their data can be fitted by

$$\begin{aligned} T^*_{\text{freez}}(\kappa^*) &= 0.009 + 0.030286\kappa^* - 0.009964\kappa^{*2} \\ &\quad + 0.0033477\kappa^{*3} - 0.0002452\kappa^{*4} \end{aligned} \tag{8.28}$$

such that everything is explicitly known in Eq. (8.26). Equation (8.26) stems from 40 BD simulations for different parameters scanning the whole fluid regime from $\kappa^* = 0$ (unscreened plasma interaction) to 7. It contains a small relative error of 4% for $0 \le \kappa^* \le 7$.

At the freezing transition we have $t_r \equiv 1$, and only the first exponential in Eq. (8.26) gives a relevant contribution such that we see directly the universality of D_L/D_0 with respect to κ^*, where the actual value is $D_L/D_0 = 0.098$.

8.3.4 Dynamical Test of the Effective Interaction between Colloidal Particles

Equation (8.26) was used to analyze experimental data for D_L/D_0 obtained from forced Rayleigh scattering experiments on charged suspensions with varying salt and particle concentrations [69], which then provides a *dynamical test* of the particle interactions. Two different theoretical Yukawa models were tested against the experimental results: the DLVO model defined by Eqs. (8.2)–(8.4), and the Poisson-Boltzmann cell model [8]. The results are shown in Figs. 8.7 and 8.8. All parameters of the experimental sample were known by a careful characterization of the colloidal suspension; in particular, the true bare particle charge Z was determined from other measurements to be $Z = 580$. Once the theoretical Yukawa description of the interaction is fixed, there is no free fitting parameter involved in the comparison between the experimental and simulational

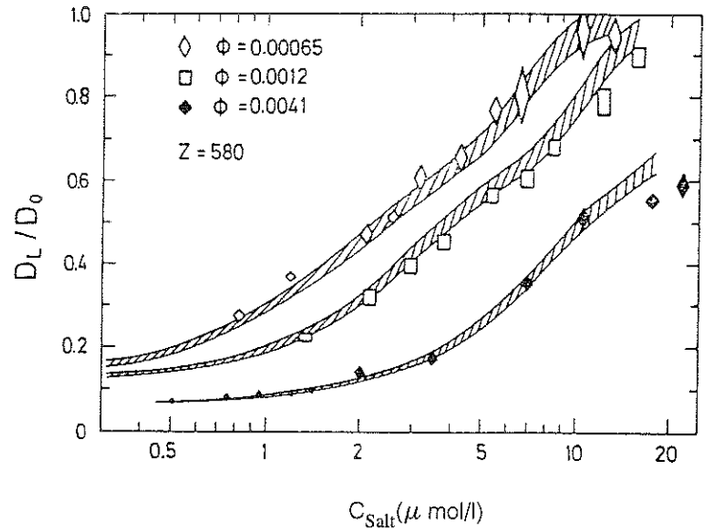

Figure 8.7 Comparison of three series of experimental data for D_L/D_0 with Eq. (26) for the Poisson-Boltzmann-cell model for varying salt concentration c_{salt}. The bare charge is $Z = 580$. The symbols correspond to packing fractions of $\phi = 0.0041, 0.0012, 0.00065$. Hatched areas: prediction using these parameters in Eq.(8.26) with 4% uncertaincy. From Ref. [69].

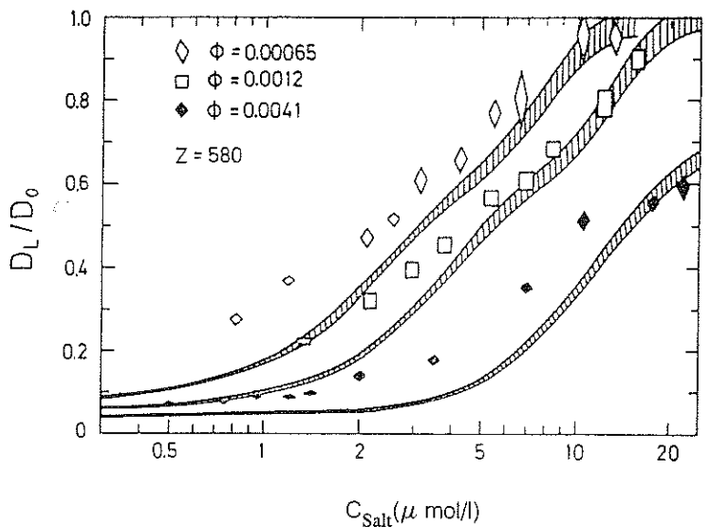

Figure 8.8 Same as Fig. 7, but now for the DLVO model. From Ref. [69].

data. The hatched area in Figs. 8.7 and 8.8 corresponds to the predictions of Eq. (8.26) within the given relative error of 4%. The symbols indicate the experimental data points for different particle concentrations n_p (or volume fractions ϕ) and varying salt concentration. One can clearly discriminate between the DLVO and the Poisson-Boltzmann-cell model. As expected, the DLVO model fails since the particles are highly interacting, while the description of the Poisson-Boltzmann-cell model gives remarkably good agreement with the experimental data. Again we emphasize that there is no fit parameter involved. Consequently the nature of the direct effective interparticle forces can be obtained from *dynamical* measurements. The usual route consistes of a comparison with the liquid structure factor $S(Q)$ (see, e.g., [72]. This quantity, however, is drastically affected by charge and size polydispersity [73]. The advantage of the dynamical test of the interaction potentials is that long-time self-diffusion, on the other hand, is rather sensitive to the interparticle forces but rather insensitive to polydispersity effects.

We finally remark that there are further theoretical Yukawa models for the effective interaction between charged colloidal suspensions. Belloni [74] has solved the mean-spherical approximation (MSA) of the primitive model analytically where one also ends up with an effective Yukawa interaction. The result is very close the DLVO potential. Within the experimental error of the data from Ref. [69], one cannot see a big difference between the MSA and the DLVO potential. Thus the MSA model fails as the DLVO model does. Second, there is a modified DLVO approximation that is empirically justified for strongly interacting particles [50]. This Yukawa potential, in turn, is very close to the Poisson-Boltzmann-cell model and is capable of describing the experimental data well.

8.4 Self-Diffusion in Liquid-Crystalline Systems

In this section we study the long-time diffusion of rodlike particles; that is, we are dealing with *anisotropic* liquids. In this case one has translational and rotational long-time diffusion, which are investigated in the framework of a simple model of hard spherocylinders [70]. In order to keep the model simple, we consider Brownian dynamics of hard spherocylinders neglecting hydrodynamic interactions. The spherocylinders have a total width L_c and diameter d_c, and a rod configuration is characterized by its center-of-mass coordinates $\{\mathbf{R}_i : i = 1, \ldots, N\}$ and orientations $\{\mathbf{\Omega}_i : i = 1, \ldots, N\}$, where $\mathbf{\Omega}_i$ is a unit vector. The potential energy is simple a excluded-volume type: It is zero if the rods do not overlap and infinite otherwise. Due to this simple interaction, the temperature T scales out and the rod number density n_p is the only thermodynamic variable. This density is conveniently expressed in terms of the rod packing fraction $\phi = n_p \pi d_c^2 [d/6 + (L_c - d_c)/4]$. Choosing the rod diameter d_c as the typical length scale, the only additional geometric quantity is the length-to-width ratio

$$p_c = L_c/d_c \tag{8.29}$$

of the rods. Hence all structural and thermodynamic quantities including the bulk phase diagram only depend on ϕ and p_c. For $L_c = d_c$ the isotropic case of hard spheres is recovered.

We adopt Brownian dynamics of the rods and approximate the short-time dynamics by that of one single rod in a solvent characterized by two translational short-time diffusion constants, $D^{\perp}$ and $D^{\parallel}$, perpendicular and parallel to the rod axis, and a rotational short-time diffusion constant D^r. As a function of p_c, these three diffusion constants have been calculated by Broersma [75] and Tirado et al. [76, 77]:

$$D^{\perp} = \frac{D_0^*}{4\pi}(\ln p_c + 0.839 + 0.185/p_c + 0.233/{p_c}^2) \tag{8.30}$$

$$D^{\parallel} = \frac{D_0^*}{2\pi}(\ln p_c - 0.207 + 0.980/p_c - 0.133/{p_c}^2) \tag{8.31}$$

$$D^r = \frac{3D_0^*}{\pi L_c^2}(\ln p_c - 0.662 + 0.917/p_c - 0.050/p_c^2) \tag{8.32}$$

with

$$D_0^* = k_B T/\eta L_c \tag{8.33}$$

where η the shear viscosity of the solvent.

The corresponding finite difference equations for Brownian dynamics of rods are a bit more complicated than Eq. (8.5) for spheres. At a given time t, the center-of-mass position $\mathbf{R}_i(t)$ of the ith rod can be split into a part $\mathbf{R}_i^{\parallel}(t) \equiv [\mathbf{\Omega}_i(t) \cdot \mathbf{R}_i(t)]\mathbf{\Omega}_i(t)$ parallel and another part $\mathbf{R}_i^{\perp}(t)$ perpendicular to the rod orientation $\mathbf{\Omega}_i(t)$ such that

$$\mathbf{R}_i(t) = \mathbf{R}_i^{\parallel}(t) + \mathbf{R}_i^{\perp}(t) \tag{8.34}$$

The same separation into a parallel and perpendicular part can be done for the total force $\mathbf{F}_i(t)$, acting on the ith rod due to the interaction with the other rods

$$\mathbf{F}_i(t) = \mathbf{F}_i^{\parallel}(t) + \mathbf{F}_i^{\perp}(t) \tag{8.35}$$

Then for a finite time step Δt the temporal evolution of $\mathbf{R}_i(t)$ is given by

$$\mathbf{R}_i^{\parallel}(t + \Delta t) = \mathbf{R}_i^{\parallel}(t) + \frac{D^{\parallel}}{k_B T}\mathbf{F}_i^{\parallel}(t)\,\Delta t + (\Delta R^{\parallel})_R \mathbf{\Omega}_i(t) \tag{8.36}$$

where $(\Delta R^{\parallel})_R$ is a random displacement due to solvent kicks, which is a Gaussian-distributed random number with zero mean, $\overline{(\Delta R^{\parallel})_R} = 0$, and variance

$$\overline{(\Delta R^{\parallel})_R^2} = 2D^{\parallel}\,\Delta t \tag{8.37}$$

The perpendicular part, on the other hand, diffuses with the perpendicular diffusion constant $D^{\perp}$:

$$\mathbf{R}_i^{\perp}(t + \Delta t) = \mathbf{R}_i^{\perp}(t) + \frac{D^{\perp}}{k_B T}\mathbf{F}_i^{\perp}(t)\,\Delta t + (\Delta R_1^{\perp})_R \mathbf{e}_{i1}(t) + (\Delta R_2^{\perp})_R \mathbf{e}_{i2}(t) \tag{8.38}$$

where again $(\Delta R_1^{\perp})_R$ and $(\Delta R_2^{\perp})_R$ are Gaussian distributed with zero mean and variance $2D^{\perp}\Delta t$. Furthermore, $\mathbf{e}_{i1}(t)$ and $\mathbf{e}_{i2}(t)$ are two orthogonal unit vectors perpendicular to $\mathbf{\Omega}_i(t)$.

Finally the orientational degree of freedom diffuses as

$$\mathbf{\Omega}_i(t + \Delta t) = \mathbf{\Omega}_i(t) + \frac{D^r}{k_B T}\mathbf{M}_i(t) \times \mathbf{\Omega}_i(t)\,\Delta t + x_1 \mathbf{e}_{i1}(t) + x_2 \mathbf{e}_{i2}(t) \tag{8.39}$$

where now $\mathbf{M}_i(t)$ is the torque acting on rod i and x_1, x_2 are Gaussian random numbers with zero mean and variance $2D^r\Delta t$.

Using this kind of Brownian motion, extensive BD simulations for the long-time translational and rotational diffusion coefficients were carried out by Löwen [70] over the whole range of the fluid phase in the (ϕ, p_c) phase diagram. The translational long-time self-diffusion coefficient D_L^t is defined as

$$D_L^t = \lim_{t\to\infty} D^t(t) \tag{8.40}$$

with

$$D^t(t) = W(t)/6t \tag{8.41}$$

where

$$W(t) = \frac{1}{N}\sum_{i=1}^{N} < [\mathbf{R}_i(t) - \mathbf{R}_i(0)]^2 > \equiv < [\mathbf{R}_1(t) - \mathbf{R}_1(0)]^2 > \tag{8.42}$$

is the mean square displacement of the center-of-mass coordinate. A natural scale for D_L^t is its short-time limit $D^t = \lim_{t\to 0} D^t(t)$ given by:

$$D^t = \tfrac{1}{3}(2D^{\perp} + D^{\parallel}) \tag{8.43}$$

The long-time orientational self-diffusion coefficient D_L^r, on the other hand, is defined via the long-time limit of a diffusive process on the unit sphere:

$$D_L^r = \lim_{t\to\infty} D^r(t) \tag{8.44}$$

with

$$D^r(t) = -\frac{1}{2t}\ln[< \Omega_1(0)\Omega_1(t) >] \tag{8.45}$$

Of course, the short-time limit $D^r = \lim_{t\to 0} D^r(t)$ provides a natural scale for $D^r(t)$.

It is tempting to check whether there are dynamical freezing rules by looking at the values of D_L^t/D^t and D_L^r/D^r at the freezing line of the liquid. The phase diagram of hard spherocylinders is known by Monte Carlo simulations of Veerman and Frenkel [78] involving stable fluid, crystalline, nematic, and smectic phases. In particular, the location of the fluid-nematic and fluid-crystalline coexistence line is known for $p_c = 1, 2, 4, 6$ [78]. For $p_c > 6$ the theory of Lee [79] gives explicit data for the coexisting fluid and nematic densities including the limit $p_c \to \infty$, which is known exactly from Onsager's theory [80–82].The Monte Carlo simulations have also revealed that the coexisting phase is crystalline for $p_c \lesssim 4.5$, whereas it is nematic for $p_c \gtrsim 4.5$.

For very high p_c ($p_c > 30$) Onsager's theory yields an asymptotically exact expression for the fluid density ϕ_f at the fluid-nematic transition [81, 82]:

$$\phi_f = 3.2906/p_c \tag{8.46}$$

Furthermore the tube model (see, e.g., Doi and Edwards [83]) yields $D_L^r/D^r = b_c(n_p L_c^3)^{-2}$, where an estimate of b_c can be obtained by fitting the simulation data of Doi et al., resulting in $b_c = 540$ [84]. This yields the asymptotic prediction

$$D_L^r/D^r = 30.8/p_c^2 \tag{8.47}$$

along the fluid-nematic transition line, which becomes valid for $p_c \gtrsim 30$. On the other hand, the translational diffusion tends to $D_L^t/D^t = \frac{1}{3}$ as $p_c \to \infty$ according to the tube model.

In Fig. 8.9, the simulational results of Löwen [70] for D_L^t/D^t and D_L^r/D^r are plotted versus $1/p_c$ for ϕ being on the fluid freezing line. Both simulational data and the asymptotic formula Eq. (8.47) are shown. It turns out that along the freezing line both D_L^t/D^t and D_L^r/D^r are *nonmonotonic* with p_c. The translational diffusion is nonmonotonic in the crystalline region. This is connected to the nonmonotonicity in p_c of the coexisting fluid packing fraction ϕ_f. In the nematic region, D_L^t/D^t increases monotonically to its "tube limit" 1/3. This limit is practically reached for $p_c \gtrsim 10$.

On the other hand, D_L^r/D^r is strongly decreasing for small increasing p_c in the crystalline region. Then, for $2 \le p_c \le 6$, it stays more or less constant ≈ 0.12 irrespective of whether the coexisting phase is crystalline or nematic. If p_c is increased further, D_L^r/D^r increases again and then decreases approaching its asymptotic law given by Eq. (8.47) for $p_c \gtrsim 20$.

Hence it becomes clear that both diffusion ratios D_L^t/D^t and D_L^r/D^r vary significantly along the freezing line, both in the crystalline and nematic region. Consequently a simple universal dynamical freezing criterion that would guarantee a universal value of D_L^t/D^t or D_L^r/D^r for arbitrary p_c is missing. Nevertheless, in the relatively broad region $2 \le p_c \le 6$ where the coexisting phase may be crystalline or nematic, D_L^r/D^r is roughly constant. This is the rotational analog of the dynamical freezing rule for spherical systems: It states that *an anisotropic fluid freezes if its long-time rotational self-diffusion coefficient is one order of magnitude smaller than its short-time limit.*

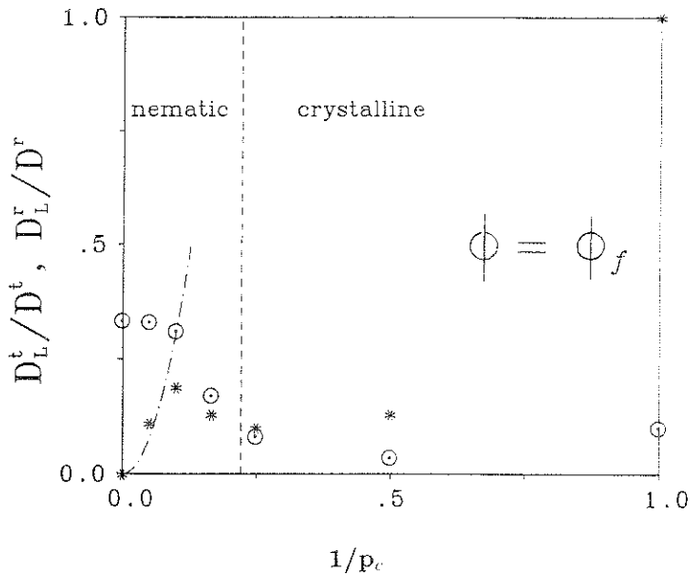

Figure 8.9 Translational and rotational long-time diffusion coefficients, D_L^t (circles) and D_L^r (stars), measured in terms of their short-time limits, D^t and D^r, versus $1/p_c$ at coexistence of the liquid with the crystalline or nematic phase. The dot-dashed line is the asymptotic law Eq. (8.47). The dashed line separates the nematic and crystalline region. From Ref. [70].

8.5 Some Further Open Problems

Let us finally list some fascinating open problems that are relevant to the context of dynamics of colloidal suspensions across the freezing and glass transition. They are mainly connected to systems with reduced geometry.

1. The kinetic glass transitions has not yet been studied in detail for a fluid *confined* to pores or between plates. It is expected that boundaries strongly influence the location of the kinetic glass transition point. If crystallization at the walls can be circumvented, the glass transition should occur at much higher temperatures than in the bulk fluid if the dimensions of the sample (the pore diameter or the distance between the plates) is comparable to the mean interparticle spacing ℓ [85, 86]. Recently, Fehr and Löwen [87] have considered a soft-sphere mixture between two parallel plates. In order to avoid wall crystallization, a lateral disorder was introduced on the walls. The corresponding bulk kinetic glass transition was extensively investigated by Roux, Barrat, and Hansen [88, 89]. The preliminary results indicate a shift of the glass transition temperature to significantly larger values as compared to the bulk glass transition known from Refs. [88] and [89]. Up to now, there

has been no attempt to perform a simple mode-coupling theory in restricted geometry to study the shift of the glass transition theoretically. This is a challenging problem for the future.

2. If the distance between parallel charged plates confining a charged colloidal suspension is enhanced or the surface charge is increased, one finally ends up with a quasi-two-dimensional system. The fundamental question arises whether the kinetic glass transition in two spatial dimensions is fundamentally different from that in three dimensions or not. Recent computer simulational results for a two-dimensional Lennard-Jones liquid by Ranganathan [90] indicate that the qualitative scenario in two dimensions is qualitative similar to that in three dimensions. This is different from the freezing and melting transition, which is definitively different in two dimensions. One should also do quantitative comparison with mode-coupling theory in this case.
3. What about a dynamical freezing rule in two dimensions? Recent investigations of Grier and Murray [5] studying the nonequilibrium formation of quasi-two-dimensional crystal indicate that it is fulfilled in 2D. The fundamental problem is that the nature of the freezing transition is still not completely clear in two dimensions. This concerns mainly the existence of a hexatic phase with long-range orientational order that would intervene between the fluid and solid phase. Strictly speaking [91] there is no translational long-range order in two dimensions, and consequently a crystal phase with long-range order is not thermodynamically stable.

For quasi-two-dimensional colloidal fluids a Yukawa interaction is an approximate description of the interaction, and Brownian dynamics simulations have been performed to get the long-time self-diffusion coefficients by Löwen [92]. In contrast to molecular dynamics in two dimensions, where the long-time self-diffusion coefficient diverges, it is finite for 2D Brownian dynamics.

Another problem is how to locate the fluid coexistence line exactly. Recent simulations with the 2D Yukawa potential by Naidoo and Schnitker [93] are still too inconclusive to decide the exact phase behavior in two dimensions.

4. The glass transition in liquid crystals is more complicated. To date no computer simulation has been reported observing a fluid phase with slow dynamics. Apparently nematic phase formation is fast enough to exclude a glass transition. More detailed work from theory, experiments, and computer simulations is needed to study the slowing down of translational and orientational motion in compressed or supercooled anisotropic fluids.
5. Excellent realizations of charged colloidal rodlike systems are aqueous suspensions of tabacco mosaic viruses. Recently it was shown by Löwen [94] by using an "ab initio" calculation that the Yukawa segment model originally introduced by Klein and co-workers [95, 96] (see also Ref. [97]) is a good description of the interaction. There is a considerable need to explore the complete phase diagram of the Yukawa segment model by computer simulation or density-functional theory and to investigate time-dependent correlation functions by Brownian dynamics simulations. One first step in this direction

was done by Kirchhoff et al., who calculated long-time orientational and translational self-diffusion for the Yukawa segment model [98].

Acknowledgements

I thank J. P. Hansen, P. A. Madden, G. Szamel, T. Kirchhoff, R. Klein, T. Palberg, and J.-L. Barrat for helpful discussions. This work was supported by the Bundesministerium für Forschung und Technologie (BMFT) under Contract No. 03-WA3LMU.

References

1. Russel, W. B., Saville, D. A., and Schowalter, W. R., *Colloidal Dispersions* (Cambridge University Press, Cambridge, 1989).
2. Pusey, P. N., in *Liquids, Freezing and the Glass Transition*, Eds. J.P. Hansen, D. Levesque, and J. Zinn-Justin (North Holland, Amsterdam, (1991), p. 763.
3. Sood, A. K., in *Solid State Physics*, Eds. H. Eherenreich and D. Turnbull (Academic, New York) **45**, 1 (1991).
4. Löwen, H., Physics Reports **237**, 249 (1994).
5. Grier, D. G., and Murray, C. A., in *Structure and Dynamics of Strongly Interacting Colloids and Supramolecular Aggregates in Solution*, Eds. S. H. Chen, J. S. Huang, and P. Tartaglia (Nato ASI, Kluwer, 1992), p. 145.
6. Derjaguin, B. V., and Landau, L. D., *Acta Physicochim. USSR* **14**, 633 (1941).
7. Verwey, E. J. W., and Overbeek, J. Th., *Theory of the Stability of Lyophobic Colloids* (Elsevier, Amsterdam, 1948).
8. Alexander, S., Chaikin, P. M., Grant, P., Moraes, G. J., Pincus, P., and Hone, D., *J. Chem. Phys.* **80**, 5776 (1984).
9. Löwen, H., Maden, P. A., and Hansen, J. P., *Phys. Rev. Lett.* **68**, 1081 (1992).
10. Löwen, H., Hansen, J. P., and Madden, P. A., *J. Chem. Phys.* **98**, 3275 (1993).
11. Löwen, H., and Kramposthuber, G., *Europhys. Lett.* **23**, 673 (1993).
12. Ermak, D. L., *J. Chem. Phys.* **62**, 4189, 4197 (1975).
13. Allen, M. P., and Tildesley, D. J., *Computer Simulation of Liquids* (Clarendon Press, Oxford, 1987).
14. Löwen, H., Roux, J. N., and Hansen, J. P., *J. Phys. Condens. Matter.* **3**, 997 (1991).
15. Löwen, H., Palberg, T., and Simon, R., *Phys. Rev. Letts.* **70**, 1557 (1993).
16. Lindemann, F. A., *Phys. Z.* **11**, 609 (1910).
17. Hansen, J. P., and Verlet, L., *Phys. Rev.* **184**, 151 (1969).
18. Pusey, P. N., and van Megen, W., *Phys. Rev. Lett.* **59**, 2083 (1987).
19. Pusey, P. N., and van Megen, W., *Phys. Rev.* **A 43**, 5429 (1991).
20. van Megen, W., Underwood, S. M., and Pusey, P. N., *Phys. Rev. Lett.* **67**, 1586 (1991).
21. van Megen, W., and Underwood, S. M., *Phys. Rev. Lett.* **70**, 2766 (1993).
22. van Megen, W., and Underwood, S. M., *Phys. Rev.* **E 47**, 248 (1993).
23. Bartsch, E., Antoinetti, M., Schupp, W., and Sillescu, H., *J. Chem. Phys.* **97**, 3950 (1992).
24. Bartsch, E., Frenz, V., Möller, S., and Sillescu, H., *Physica A* **201**, 363 (1993).
25. Sillescu, H., and Bartsch, E., in *Disorder Effects on Relaxational Processes*, Eds. R. Richert and A. Blumen (Springer, Berlin, 1993), p. 59.
26. Sirota, E. B., Ou-Yang, H. D., Sinha, S. K., Chaikin, P. M., Axe, J. D., and Fuji, Y., *Phys. Rev. Lett.* **62**, 1524 (1989).
27. Meller, A., and Stavans, J., *Phys. Rev. Lett.* **68**, 3646 (1992).
28. Götze, W., in *Liquids, Freezing and the Glass Transition*, Eds. J.P. Hansen, D. Levesque, and J. Zinn-Justin (North Holland, Amsterdam, 1991), p. 287.
29. Götze, W., and Sjögren, L., *Phys. Rev.* **A 43**, 5442 (1991).

30. Fuchs, M., Hofacker, I., and Latz, A., *Phys. Rev.* **A 45**, 898 (1992).
31. Szamel, G., and Löwen, H., *Phys. Rev.* **A 44**, 8215 (1991).
32. Fuchs, M., private communication, 1993.
33. Kawasaki, K., *Physica A* **208**, 35 (1994).
34. Löwen, H., Hansen, J. P., and Roux, J. N., *Phys. Rev.* **A 44**, 1169 (1991).
35. Baschnagel, J., Binder, K., and Wittmann, H. -P., *J. Phys. Condens. Matter* **5**, 1597 (1993).
36. Kob, W., and Anderson, H. C., *Phys. Rev.* **E 47**, 3281 (1993).
37. Kob, W., and Anderson, H. C., *Phys. Rev.* **E 48**, 4364 (1993).
38. Migayawa, H., Hiwatari, Y., Bernu, B., and Hansen, J. P., *J. Chem. Phys.* **88**, 3879 (1988).
39. Löwen, H., and Hansen, J. P., in *Recent Developments in the Physics of Liquids*, Eds. W. S. Howells and A. K. Soper (IOP Publishing, Bristol, 1991), p. F283.
40. Walrand, S., Belloni, L., and Drifford, M., *J. Physique* **47**, 1565 (1986).
41. Kops-Werkhoven, M. M., and Fijnaut, H. M., *J. Chem. Phys.* **77**, 2242 (1982).
42. Kops-Werkhoven, M. M., Pathmamanoharan, C., Vrij, A., and Fijnaut, H. M., *J. Chem. Phys.* **77**, 5913 (1982).
43. Ottewill, R. H., and Williams, N. St. J., *Nature (London)* **325**, 232 (1987).
44. van Veluwen, A., and Lekkerkerker, H. N. W., *Phys. Rev.* **A 38**, 3758 (1988).
45. van Megen, W., and Underwood, S. M., *J. Chem. Phys.* **91**, 552 (1989).
46. Dergiorgio, V., Piazza, R., Corti, M., and Stavans, J., *J. Chem. Soc. Faraday Trans.* **87**, 431 (1991).
47. van Megen, W., Underwood, S., Ottewill, R., Williams, N., and Pusey, P. N., *J. Chem. Soc. Faraday Discuss.* **83**, 47 (1987).
48. Härtl, W., Versmold, H., Wittig, U., and Linse, P., *J. Chem. Phys.* **97**, 7797 (1992).
49. Härtl, W., Versmold, H., and Zhang-Heider, X., *Ber. Bunsenges. Phys. Chemie* **95**, 1105 (1991).
50. Dozier, W. D., Lindsay, H. M., and Chaikin, P. M., *J. de Physique, Colloque* **C3**, 165 (1985).
51. Simon, R., Palberg, T., and Leiderer, P., *J. Chem. Phys.* **99**, 3030 (1993).
52. van Blaaderen, A., Peetermans, J., Maret, G., and Dhont, J. K. G., *J. Chem. Phys.* **96**, 4591 (1992).
53. Imhof, A., van Blaaderen, A., Maret, G., Mellema, J., and Dhont, J. K. G., *J. Chem. Phys.* **100**, 2170 (1994).
54. Wiese, H., and Horn, D., *J. Chem. Phys.* **94**, 6429 (1991).
55. Bless, M. H., and Leyte, J. C., *J. Coll. Interfac. Science* **157**, 355 (1993).
56. Zwanzig, R., *Ann. Rev. Phys. Chem.* **16**, 67 (1965).
57. Hess, W., and Klein, R., *Adv. Phys.* **32**, 173 (1983).
58. Klein, R., and Hess, W., in *Ionic Liquids, Molten States and Polyelectrolytes*, Eds. K. H. Bennemann, F. Bouers, and D. Quitmann; Lecture Notes in Physics **172**, 199 (1982).
59. Nägele, G., Medina-Noyola, M., Klein, R., and Arauz-Lara, J. L., *Physica A* **149**, 123 (1988).
60. Medina-Noyola, M., *Phys. Rev. Lett.* **60**, 2705 (1988).
61. Hansen, J.-P., and McDonald, I. R., *Theory of Simple Liquids*, 1st edn. (Academic Press, London, 1976).
62. Cichocki, B., *Physica A* **148**, 165 (1988); **148**, 191 (1988).
63. Löwen, H., and Szamel, G., *J. Phys. Condens. Matter* **5**, 2295 (1993).
64. Leegwater, J. A., and Szamel, G., *Phys. Rev.* **A 46**, 4999 (1992).
65. Szamel, G., and Leegwater, J. A., *Phys. Rev.* **A 46**, 5012 (1992).
66. Indrani, A. V., and Ramaswamy, S., *Phys. Rev. Lett* **73**, 360 (1994).
67. Cichocki, B., and Hinsen, K., *Physica A* **166**, 473 (1990).
68. Cichocki, B., and Hinsen, K., *Physica A* **187**, 133 (1992).
69. Bitzer, F., Palberg, T., Löwen, H., Simon, R., and Leiderer, P., *Phys. Rev.* **E 50**, 2821 (1994).
70. Löwen, H., *Phys. Rev.* **E 50**, 1232 (1994).
71. Meijer, E. J., and Frenkel, D., *J. Chem. Phys.* **94**, 2269 (1991).
72. Härtl, W., and Versmold, H., *J. Chem. Phys.* **88**, 7157 (1988).
73. D'Aguanno, B., and Klein, R., *Phys. Rev.* **A 46**, 7652 (1992).
74. Belloni, L., *J. Chem. Phys.* **85**, 519 (1986).

75. Broersma, S., *J. Chem. Phys.* **32**, 1626 (1960); **32**, 1632 (1960); **74**, 6989 (1981).
76. Tirado, M. M., and de la Torre, J. G., *J. Chem. Phys.* **71**, 2581 (1979); **73**, 1986 (1980).
77. Tirado, M. M., Martinez, C. L., and de la Torre, J. G., *J. Chem. Phys.* **81**, 2047 (1984).
78. Veerman, J. A. C., and Frenkel, D., *Phys. Rev.* **A 41**, 3237 (1990).
79. Lee, S.-D., *J. Chem. Phys.* **87**, 4972 (1987).
80. Onsager, L., *Ann. N. Y. Acad. Sci.* **51**, 627 (1949).
81. Lasher, G., *J. Chem. Phys.* **53**, 4141 (1970).
82. Kayser, R. F., and Raveche, H. J., *Phys. Rev.* **A 17**, 2067 (1978).
83. Doi, M., and Edwards, S. F., *The Theory of Polymer Dynamics* (Oxford University Press, Oxford, 1986).
84. Doi, M., Yanamoto, I., and Kano, F., *J. Phys. Soc. Japan* **53**, 3000 (1984).
85. Hu, H.-W., Carson, G. A., and Granick, S., *Phys. Rev. Lett.* **66**, 2758 (1991).
86. Thompson, P. A., Grest, G. S., and Robbins, M. O., *Phys. Rev. Lett.* **68**, 3448 (1992).
87. Fehr, T., and Löwen, H., *Phys Rev.* **E 52**, 4016 (1995).
88. Roux, J. N., Barrat, J. L., and Hansen, J. P., *J. Phys. Condens. Matter* **1**, 7171 (1989).
89. Barrat, J. L., Roux, J. N., and Hansen, J. P., *Chem. Phys.* **149**, 197 (1990).
90. Ranganathan, S., *J. Phys. Condens. Matter* **6**, 1299 (1994).
91. Fröhlich, J., and Pfister, C., *Commun. Math. Phys.* **81**, 277 (1981).
92. Löwen, H., *J. Phys. Condens. Matter* **4**, 10105 (1992); **5**, 2649 (1993).
93. Naidoo, K. J., and Schnitker, J., *J. Chem. Phys.* **100**, 3114 (1994).
94. Löwen, H., *Phys. Rev. Lett.* **72**, 424 (1994).
95. Schneider, J., Hess, W., and Klein, R., *J. Phys. A: Math. Gen.* **18**, 1221 (1985).
96. Schneider, J., Karrer, D., Dhont, J. K. G., and Klein, R., *J. Chem. Phys.* **87**, 3008 (1987).
97. Deutsch, J. M., and Goldenfeld, N., *J. Physique* **43**, 651 (1982).
98. Kirchhoff, T., Löwen, H., and Klein, R., *Phys. Rev.* E (in press).